How to cite: *Angew. Chem. Int. Ed.* **2022,** *61,* e202205266
International Edition: doi.org/10.1002/anie.202205266
German Edition: doi.org/10.1002/ange.202205266

Synthetic Biology

Light-Activated Membrane Transport in Polymeric Cell-Mimics

Shoupeng Cao, Lucas Caire da Silva, and Katharina Landfester**

Abstract: Giant polymersomes are versatile and stable biomimetic compartments that are ideal for building cell-like systems. However, the transport of hydrophilic molecules across the membrane, which controls the function of cell-like systems, is limited by the low permeability of polymeric bilayers. Therefore, mechanisms to control the permeability of polymersomes are necessary to create functional cell-like systems. Here, we describe the design of giant polymersomes equipped with spiropyran-based permeability modulators. Photo-isomerization of the modulators leads to perturbation of the polymer membrane, resulting in increased permeability. The photoactivated polymersomes were used to construct two cell-like systems controlled by light-activated transport of hydrophilic molecules. First, we designed an enzymatic micro-reactor activated by light irradiation. Second, we constructed a hybrid coacervate-in-polymersome system that mimics the adaptive formation of biological condensates in cells.

Introduction

Over the past decade, there has been increasing interest in the development of small polymersomes as vehicles for drug delivery and of giant polymersomes as biomimetic compartments.[1] Giant polymersomes (GPs) are cell-sized vesicles (5–100 μm) that are self-assembled from synthetic amphiphilic block copolymers, exhibit mechanical stability, and are attractive candidates for mimicking the structure and functions of the biological compartments of eukaryotic cells.[2] GPs are structurally similar to lipid bilayers in the cell membrane and liposomes. A shell structure formed by the bilayer membrane encloses and protects active components and also regulates the exchange of (chemical) signals with the environment.[3] Due to the higher molecular weight of amphiphilic polymers compared to lipids, the resulting polymeric compartments are more stable than those made from lipids. Additionally, the structure and chemistry of polymers can be easily modified to create compartments with tailored properties. This makes giant polymersomes very promising as versatile biomimetic compartments for technological applications.[4]

GPs contain a confined microenvironment in which multiple active components can be encapsulated.[3a,4a] These include biomolecules, aggregates, supramolecular structures, and even other (sub)compartments, the combination of which can lead to cell-like systems with complex internal composition and increased functionality.[5] Cell-like systems, also known as synthetic cells, can mimic the hierarchical architecture of eukaryotic cells via the integration of subcompartments.[6] They can also replicate sophisticated cellular behaviors, including multistep enzymatic cascade reactions, gene expression, adaptive biochemistry, intercellular communication, and motility.[7] However, most of the processes that occur in synthetic cells constructed with GPs can only be triggered by the passive diffusion of molecules and ions across the polymer membrane.[8]

Active control of membrane permeability is an important property for synthetic cells, as it enables precise activation and modulation of internal functions that depend on substrate uptake and chemical signaling.[9] Examples of such systems include microreactors and biosensors, whose functionality depends on the transport of substrates and analytes into compartments carrying active catalytic components.[7f,10] Controlled membrane transport of materials is a desired feature of biomimetic compartments, as it allows the bottom-up fabrication of cell-like systems with increased complexity.[11] Molecular transport through polymeric membranes usually relies on passive diffusion or involves mechanisms that lead to loss of structural integrity of the compartment.[8a,12] In general, synthetic cells with active control over membrane permeability could sense environmental cues and regulate internal processes in an adaptive manner, resulting in fine control over structural complexity and functional output.[9a,11d,13]

To this end, we describe here the development of GPs with light-activated membrane permeability that was used to construct light-controlled polymeric cell mimics. First, synthetic spiropyran-based permeability modulators were developed to be integrated into the membrane of impermeable GPs (Figure 1a). Photo-isomerization of the spiropyran modulators resulted in the perturbation of the polymer membrane, allowing hydrophilic small molecules to pass. Moreover, the structural integrity of the GPs was maintained, with macromolecular cargoes retained in the aqueous interior of the compartments. To demonstrate the application of our design, a light-activated enzymatic microreactor was constructed. In this system, substrates present in

[*] Dr. S. Cao, Dr. L. C. da Silva, Prof. Dr. K. Landfester
Max Planck Institute for Polymer Research
55128 Mainz (Germany)
E-mail: silva@mpip-mainz.mpg.de
landfester@mpip-mainz.mpg.de

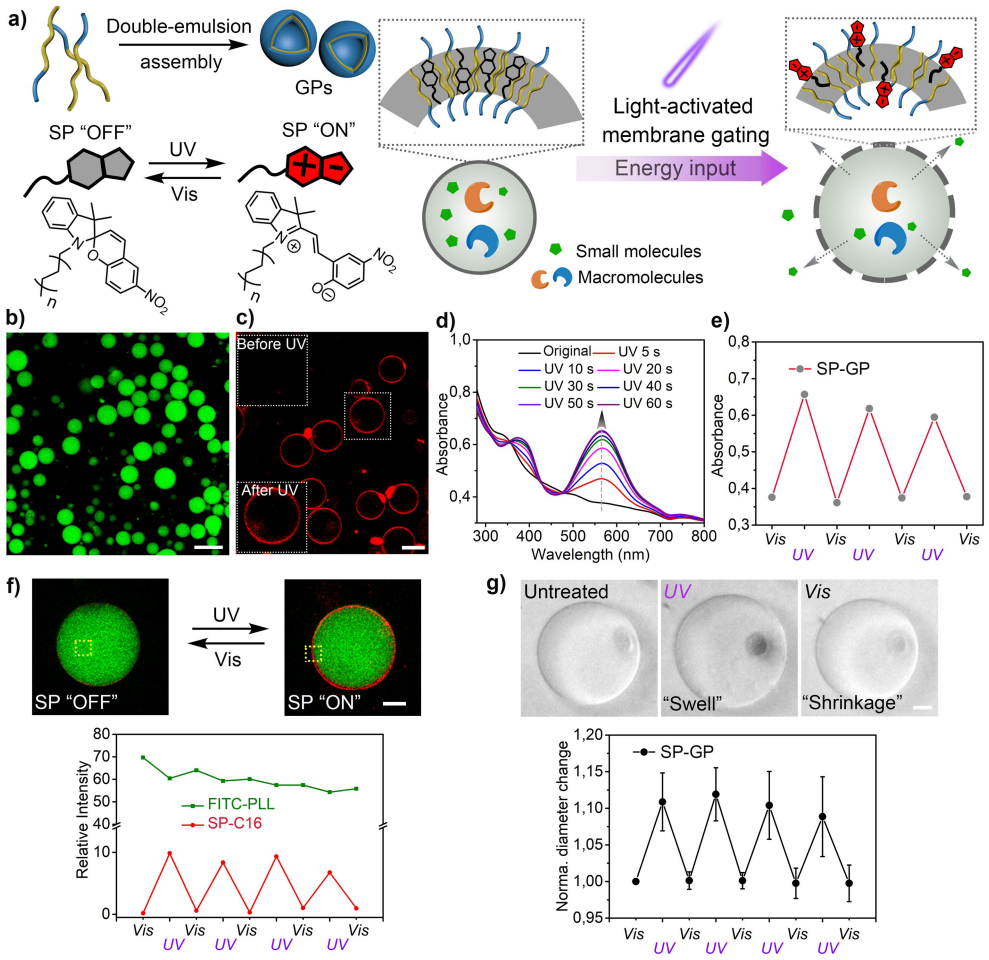

Figure 1. Design and construction of the photo-activated giant polymersomes. a) The spiropyran-embedded PB-PEO giant polymersomes were prepared via a modified double emulsion method. Upon UV-light irradiation, the fast isomerization of the spiropyran photo-transducer produces a local perturbation in the polymer membrane, resulting in reversible swelling and increased membrane permeability. b) Encapsulation of the macromolecular fluorescence probe FITC-PLL (15 kDa) demonstrates that the GPs can compartmentalize a hydrophilic cargo in the aqueous core, scale bar = 50 μm. c) Loading of a hydrophobic cargo within the membrane was confirmed by the presence of the spiropyran photo-transducer in the polymer membrane. Embedded SP-C16 initially did not show fluorescent emission. Emission was switched on (λ_{ex} = 561 nm) upon UV light irradiation (366 nm, 8 W cm^{-2}), scale bar = 20 μm. d) UV/Vis absorbance of spiropyran-embedded polymersomes (SP-GPs) before and after UV irradiation as a function of exposure time. e) Reversible change in UV/Vis absorbance intensity of SP-GPs at λ_{abs} = 560 nm produced by alternating UV/Vis irradiation (UV irradiation 1 min, Vis irradiation 2 min). f) Reversible fluorescence "SP ON" and "SP OFF" of SP-GPs membrane upon UV and Vis light irradiation, scale bar = 20 μm. g) The photo-isomerization of SP-GPs induced a reversible mechanical response. The relative size change was determined by measuring representative vesicles (n = 20), scale bar = 10 μm.

the external medium cross the membrane barrier only after permeabilization of the GPs by light irradiation, which triggered an enzyme-mediated reaction within the compartments.

To further demonstrate the versatility of our design, a hybrid coacervate-in-polymersome system was constructed to mimic the formation of biomolecular condensates in natural cells. First, a positively charged polyelectrolyte (poly-L-lysine) was loaded into the lumen of the GPs. After light irradiation, the negatively charged multivalent nucleotides (ATP) present in the external medium were able to cross the membrane barrier and diffuse into the GPs, resulting in the formation of condensates by complex coacervation. The coacervates were able to sequester and localize encapsulated proteins, resulting in a heterogeneous distribution of components within the synthetic cell. The complexity of the system was further increased by encapsulating a counter enzyme (alkaline phosphatase) to induce a time-controlled degradation of the coacervates, thus introducing transient behavior into the system. This system illustrates the high degree of activation control offered by dynamic actuation of GPs, which greatly expands the scope of biologically relevant functionalities of polymeric compartments, especially for the construction of advanced biomimetic systems.

Results and Discussion

Giant polymersomes (GPs) were obtained via a modified double emulsion method using the block copolymer poly(butadiene)-*block*-poly(ethylene oxide) (PB_{22}-b-PEO_{12}).[2d,14] The method is described in the Supporting Information. The GPs contained dextran (4 kDa, 25 mg mL^{-1}, inner concentration) dissolved in the aqueous inner phase to make them denser than the outer buffered medium (5 mM HEPES, pH 6.0). This resulted in fast sedimentation, facilitating the characterization of the vesicles by optical microscopy. The ability of the GPs to compartmentalize water-soluble molecules was demonstrated by encapsulating FITC-labelled poly-L-lysine (FITC-PLL, 15 kDa) (Figure 1b, S10).

To control the permeability of the GPs, a photo-transducer was designed to be integrated into the membrane of the GPs. The photo-transducer consisted of a photo-responsive spiropyran (SP) with a hydrophobic C_{16} tail (SP-C16) synthesized according to adapted procedures (Scheme S1).[15] The tail served as a molecular anchor to attach the photo-transducer to the polymer membrane (Figure 1a). The SP-C16 responds to light with reversible structural and electrostatic changes that depend on the wavelength of irradiation.[16] Visible light favours the spiropyran form, or "closed form" characterized by a neutral charge in neutral pH and a non-planar geometry. Upon irradiation with UV light, the C–O bond of the spiropyran breaks, resulting in the planar, conjugated merocyanine form or "open form" (Figure 1a).

Giant polymersomes with SP-C16 integrated into the membrane were then assembled, which we will refer to as SP-GP. The successful integration of SP-C16 was confirmed by the presence of the characteristic emission of the merocyanine in the vesicle membrane and loading efficiency of SP-C16 was determined by UV/Vis spectroscopy (Figure 1c, S11). The polymer membrane did not affect the intrinsic photochromic reversible response of the SP group. This was confirmed by the presence of the characteristic absorption band (500–650 nm) of the merocyanine under UV light irradiation and the corresponding disappearance of the same band under visible light (Figure 1d,e). The photo-isomerization of SP-GPs in response to UV light was also demonstrated by confocal laser scanning microscopy (CLSM) (Figure 1f). The alternation between UV and visible light produced SP-GPs in the "ON" and "OFF" states, as indicated by the characteristic red emission of the merocyanine form (Figure 1f, S12). It was expected that the large structural changes induced by photo-isomerization of SP would lead to a structural response of the polymer membrane. Indeed, photo-isomerization of SP-C16 resulted in a detectable change in vesicle size (Figure 1g). Bright-field images of SP-GPs showed that the vesicle diameter increased by about 10 % upon UV irradiation. The vesicles returned to their original size upon irradiation with visible light, which is consistent with the reversibility of the "open" and "closed" forms of the spiropyrans. The successive swelling and shrinking could be repeated over several cycles without any detectable damage to the structure and integrity of the SP-GPs (Figure 1g, S13).

The photo-isomerization of SP-C16 was found to significantly increase the membrane permeability of SP-GPs. This effect allowed small hydrophilic molecules to pass through the polymer membrane of SP-GPs only when the vesicles were exposed to a UV light pulse. Release experiments were performed with fluorescent dyes to investigate the light-induced permeabilization of SP-GPs (Figure 2a). As a control, vesicles lacking SP showed no significant release of fluorescein sodium salt (FITC-Na, MW ≈ 0.38 kDa), either in the dark or under UV light irradiation (Figure S14). In contrast, SP-GPs showed a clear release response upon UV light irradiation. About 85 % of the SP-GPs containing SP-C16 (25 wt% SP with respect to PB-PEO) lost their cargo in less than 4 min after irradiation, consistent with a time-dependent release mechanism (Figure S15). The success rate of dye release was dependent on the relative amount of SP-C16 in the SP-GPs (Figure 2d, S14). A release rate of more than 80 % was achieved with an SP-C16 content of more than 25 wt% relative to polymer weight. The successful release rate drops to 50 % at 12.5 wt% SP-C16 and to 10 % at 5 wt%. Prolonged incubation with smaller amount of SP-16 did not increase the cargo release in polymersomes (Figure S16). This trend is consistent with the formation of membrane defects through which the molecules can pass. In this case, higher amounts of phototransducers in the polymer membrane are expected to produce a stronger effect, as observed. The SP-GPs in the following discussion assumes the use of SP-C16 with the optimal content of 25 wt %.

To understand the role of the SP tail in the permeability modulation of SP-GPs, we synthesized different versions of the photo-transducers with distinct carbon chain lengths: SP-C1 (with methyl group), SP-C4 (with butyl group), and SP-C10 (with decyl group) (Figure S17).[15,17] These were prepared according to similar general procedures used for SP-C16. The effect of SP tail length on membrane permeability was measured using FITC tagged probes of different molecular weights. The release was measured by comparing the relative fluorescence intensity of the vesicles with that of the surrounding medium, as determined by microscopy imaging. The dye release profile for the smallest molecule (FITC-Na) with SP-C10 and SP-C16 was comparable, with a complete loss of contrast observed in approximately 80 % of SP-GPs within 2 min of UV irradiation (Figure 2b). We attribute the increase in permeability to the formation of membrane defects and increased hydrophilicity caused by photo-isomerization of the spiropyran.

UV light triggers the conversion of the spiropyran from the closed to the open form. This transition is accompanied by a strong increase in local hydrophilicity and charge, which is the driving force for the appearance of local defects in the polymer membrane.[16] A dye release success rate of less than 100 % suggests that vesicle permeabilization was not homogeneous across the different SP-GPs. We hypothesize that this was caused by the distinct photochromic properties of the spiropyran derivatives and some degree of randomness in the orientation of the spiropyrans in the polymer

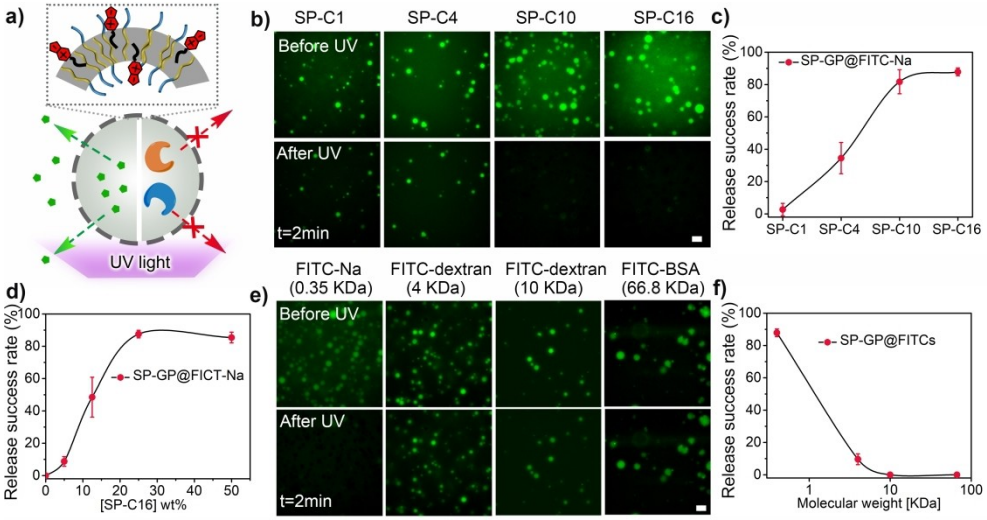

Figure 2. Light-induced permeabilization of SP-GP and size-selective release of internal molecules. a) Cartoon representation of the light-induced change in permeability of SP-GP. Activation by UV light results in SP-GP with high permeability to small molecules (in green). Macromolecular cargoes are effectively retained. b) Light-induced release of small molecules (FITC-Na) from SP-GP. Data show the first and last image of scanned images acquired within 2 min (5 s per scan). Each image was acquired immediately after a short UV pulse (approximately 0.4 s) with a fluorescence microscope. The effect of SP tail length is shown. Cargo release is indicated by the loss of internal fluorescence, scale bar = 50 μm. c) Quantification of the light-induced release of FITC-Na in SP-GPs with different SP derivatives (e.g., 25 wt. % SP with respect to PB-PEO). d) Effect of SP-C16 content on the extent of the light-induced release. e) Size-selective transport: small molecules (FITC-Na) can pass through the membrane of SP-GPs (with SP-C16). No significant release was observed for cargoes with higher molecular weight (≥ 4 kDa), scale bar = 50 μm. f) Quantification of cargo release as a function of molecular weight with SP-C16.

membrane (Figure S18). This hypothesis is supported by the observation that the shorter the SP tail, the lower the measured success rates of dye release (Figure 2c, S17). Shorter tails are expected to contribute to a more random orientation of the photo-transducer in the vesicle membranes.[17]

Spiropyrans are also pH sensitive. SP-GPs were found to rupture and irreversibly disintegrate upon UV light at low pH values (≈3.0), leading to the full release of the encapsulated materials (Nile Red and FITC-BSA) (Figure S19, S20), possibly due to the protonation of the merocyanine isomer. The protonation of the phenolic oxygen generates positively charged merocyanines. The resulting build-up of electrostatic forces results in the disintegration of vesicles at a low pH value.

Next, we investigated the effect of molecular size on membrane transport properties. SP-GPs containing high molecular weight cargoes, such as FITC-BSA (66.8 kDa) and FITC-dextran (10 kDa), showed a negligible dye release (Figure 2e, S21, S22) under UV light irradiation. Medium-sized macromolecules (4 kDa) were also retained, although some release was observed in a few vesicles (Figure 2f). In contrast, significant dye release was observed in ≈90 % of the SP-GPs with smaller molecules, FITC-Na (0.35 kDa). These results suggest that the defects created by photoisomerization of SP-C16 enable membrane transport of low molecular weight compounds. In contrast, macromolecular cargoes were too large to pass through the membrane defects and were effectively retained within the compartments.

Transport through the membrane of the SP-GPs takes place in two directions. Molecules of suitable size present in the external medium can also penetrate the polymer membrane and diffuse into the internal aqueous phase of SP-GPs (Figure 3a). Figure 3b shows CLSM images of SP-GPs in aqueous media containing distinct molecules: FITC-Na, calcein, or sulforhodamine 101. As expected, the SP-GPs were not permeable before activation by UV light (Figure 3b). After 20 s of UV light irradiation, all three molecule types were rapidly taken up (within 2 min) by the SP-GPs (Figure 3b). The integrity of the SP-GPs was not affected during this process, as shown by the fluorescence of the merocyanines in the polymer membrane (Figure 3c). However, larger macromolecules (≥ 4 kDa) could not pass through the polymer membrane (Figure 3d). These results are consistent with the controlled release experiments discussed previously.

Having demonstrated the membrane transport properties of SP-GPs, we turned our attention to the possibility of using them to construct light-activated microreactors. We expected that SP-GPs could be used to control the transport of external substrates by light while retaining large enzymes as internal catalysts. A micro-reactor was constructed using the enzyme β-galactosidase (β-gal). The enzyme was loaded into SP-GPs via the double emulsion method. β-galactosidase catalyzes the hydrolysis of fluorescein di(β-d-galactopyranoside) (β-gal-FITC, MW ≈ 0.66 kDa), a pro-fluorescent substrate that generates a fluorescent product, FITC (MW ≈ 0.33 kDa) (Figure 4a).

SP-GPs microreactors loaded with β-gal were placed in a solution containing the non-fluorescent substrate β-gal-FITC

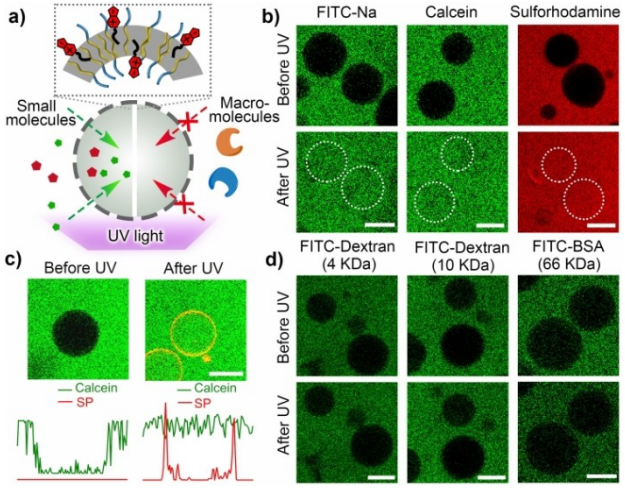

Figure 3. Selective uptake of external compounds by SP-GPs. a) Illustration shows the permeabilization of SP-GP by UV light, which allows the diffusion of small molecular cargoes into the vesicles. Macromolecules are too large to cross the membrane defects created by the photo-transducer and cannot be internalized. b) Small external substrates (FITC-Na, Calcein, and Sulforhodamine 101) can effectively cross the membrane and diffuse into the inner aqueous phase of the SP-GPs, scale bar = 20 μm. c) The fluorescence of SP-C16 (yellow contour) in the SP-GPs confirmed that the vesicles remained intact during the molecular transport of calcein. d) Large compounds with a molecular weight ≥ 4 kDa cannot penetrate the membrane of SP-GPs, scale bar = 20 μm.

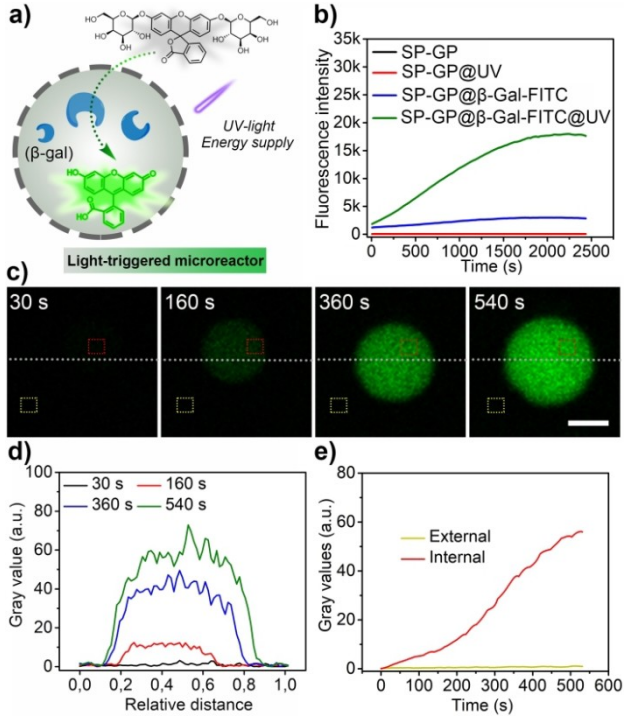

Figure 4. SP-GPs were utilized to construct light-triggered microreactors. a) UV-induced uptake of the non-fluorescent substrate (β-Gal-FITC). Enzyme-mediated hydrolysis produced an internal fluorescent output. b) Fluorescence intensity (λ_{ex} = 488 nm) of SP-GPs microreactors under different conditions: dark/UV and with/without β-Gal-FITC (0.04 mg mL^{-1}). The black and red curves overlap. The concentration of β-Gal in the inner solution was 0.05 U μL^{-1}. c) Time-lapse confocal images of SP-GP microreactors after 20 s UV irradiation in the presence of external substrate (0.1 mg mL^{-1} β-Gal-FITC), scale bar = 10 μm. d) Line profile showing the fluorescence intensity of the reaction product (FITC) in the microreactor shown in (c). e) Comparison of the fluorescence intensity inside and outside the SP-GP microreactor shown in c).

(0.04 mg mL^{-1}). After irradiation with UV light for 20 s, the fluorescence intensity (at λ_{em} = 520 nm) in the microreactors gradually increased as the reaction progressed (Figure 4b, S23, S24). As expected, the reaction only started after the SP-GP microreactors were irradiated with UV light. Time-dependent confocal laser scanning microscopy confirmed the confinement of the enzymatic reactions in the SP-GP microreactors (Figure 4c). The fluorescence intensity profiles showed a homogeneous distribution of the reaction product within the microreactors (Figure 4d, S25). Measurements of the average fluorescence intensity inside and outside the SP-GPs confirmed that the amount of product released into the external medium was minimal (Figure 4e). These results indicate that SP-GPs can be used as smart compartments in the development of light-activated microreactors.

Coacervate condensates are compartments without a physical membrane formed by liquid-liquid phase separation of oppositely charged polyelectrolytes (e.g. polymers, proteins, nucleic acids).[18] Coacervate droplets are able to sequester and concentrate active components (e.g., proteins and enzymes) in their densely packed environment, a property used by natural cells to control various biological processes.[19] Although the formation of coacervates is a straightforward process, the dynamic control of this process in multi-compartment systems remains a challenge.[6f,20]

We now demonstrate that SP-GPs equipped with adaptive membrane permeability can be used as an ideal platform for the light-activated formation of internal coacervate subcompartments. To do that, the positively charged poly-lysine polymer (2.5–20 mg mL^{-1} PLL, MW 15–30 kDa) was first encapsulated inside the SP-GPs together with fluorescently labeled PLL (10 % FITC-PLL relative to PLL, MW 15–30 kDa), while the negatively charged ATP molecules (0.1–2 mg mL^{-1}, MW ≈ 0.51 kDa) were present in the surrounding medium (Figure 5a). In this scenario, coacervates are expected to form when PLL and ATP share the same microenvironment in the SP-GPs. As a control, in the samples that were not irradiated with UV light, the formation of coacervate droplets was detected only in a few vesicles (< 5 %) even after prolonged incubation (Figure 5c and S26), which was attributed to nonspecific membrane defects. In contrast, the formation of coacervate droplets inside SP-GPs started immediately after 20 s of UV irradiation (Figure 5b), consistent with the transport of ATP into the SP-GPs. The onset and progression of coacervation could be clearly observed in most vesicles (> 90 %). The process was completed after approximately 1 min, indicating the efficient formation of internal subcompartments.

The size of the coacervate droplets formed inside the SP-GPs was measured and quantified. As shown in Figure 5d

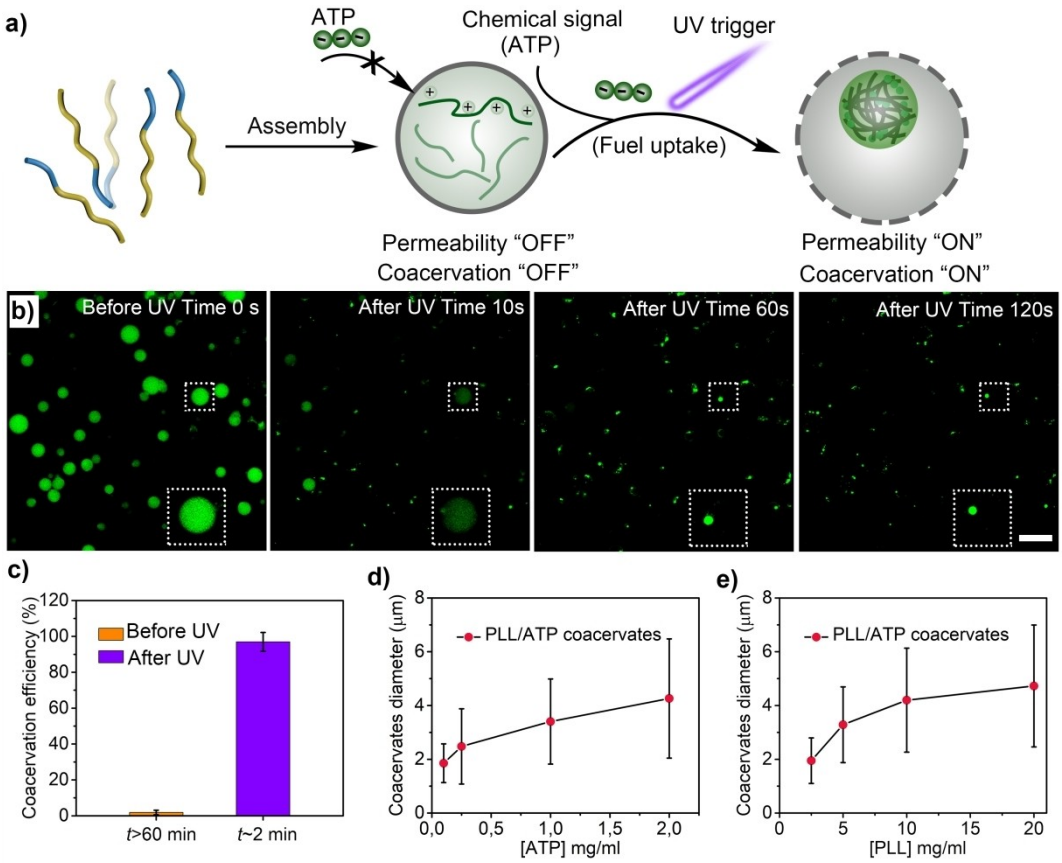

Figure 5. Light-triggered formation of sub-compartments inside SP-GPs. a) Cartoon illustration of the light-triggered formation of coacervate-in-polymersome. The external chemical signal (ATP) cannot initially cross the vesicle membrane. Upon UV irradiation, the enhanced SP-GP permeability enables the crossing of ATP into the aqueous lumen of the vesicles, inducing the condensation of poly-L-lysine (PLL) and the formation of internal coacervate droplets. b) Time-lapse confocal microscopy images of fluorescently labeled PLL present inside SP-GPs. The external solution contained 1 mg mL^{-1} ATP. Images show the progress of coacervation after 20 s of UV irradiation. Scale bar: 50 μm. c) Relative coacervation efficiency with and without UV irradiation (20 s UV irradiation). d) Effect of ATP concentration on the diameters of coacervate droplets formed inside SP-GPs (10 mg mL^{-1} PLL). e) Effect of internal initial PLL concentration on the diameter of coacervates inside SP-GPs (2.0 mg mL^{-1} external ATP).

and e, the average diameter of the coacervate subcompartments increased when the amount of either component, PLL or ATP, was increased. The diameters could be adjusted between about 2 and 4 μm depending on the concentration of the coacervate precursors. As in the previous uptake and release experiments, the coacervation process inside the SP-GP did not affect the integrity of the vesicles. This was confirmed by the presence of the SP-C16 signal in the vesicle membrane and by further membrane staining with Nile red (Figure S27). In contrast, the distribution of FITC-PLL molecules in SP-GPs changed significantly as a result of the coacervation process (Figure S27). Before UV irradiation, FITC-PLL was uniformly distributed in the SP-GPs. After UV irradiation, FITC-PLL was efficiently sequestered by the coacervate droplets, as indicated by the preferential concentration of FITC-PLL in individual small patches within the SP-GPs (Figure S27). Moreover, there is no significant sequestration behavior of dextran (FITC-labeled) in the coacervates formed inside the vesicles or in the bulk, indicating that the internal composition of the SP-GPs did not alter the coacervation process, highlighting the robustness of the coacervate formation (Figure S28/S29).

SP-GPs not only provide the ability to control the onset of the coacervation process but can also be used to spatially determine which vesicles in a population will form sub-compartments. Spatially and temporally regulated compartmentalization is a critical property of cells that can greatly expand the technological applications of biomimetic systems. Figure 6a shows confocal microscopy images of SP-GPs distributed inside and outside a rectangular area irradiated with UV light. The areas outside the rectangle were not irradiated with UV light. The results show that coacervation occurred only in vesicles located inside the UV light irradiated region. Vesicles outside the rectangular area (without UV irradiation) showed no significant formation of coacervate droplets.

Like biomolecular condensates in cells, coacervate droplets can be used as membrane-less compartments to concentrate biomolecules. This property was explored using Alexa Fluor® 647-labeled bovine serum albumin (BSA AF-647) as a model protein. Control experiments in bulk

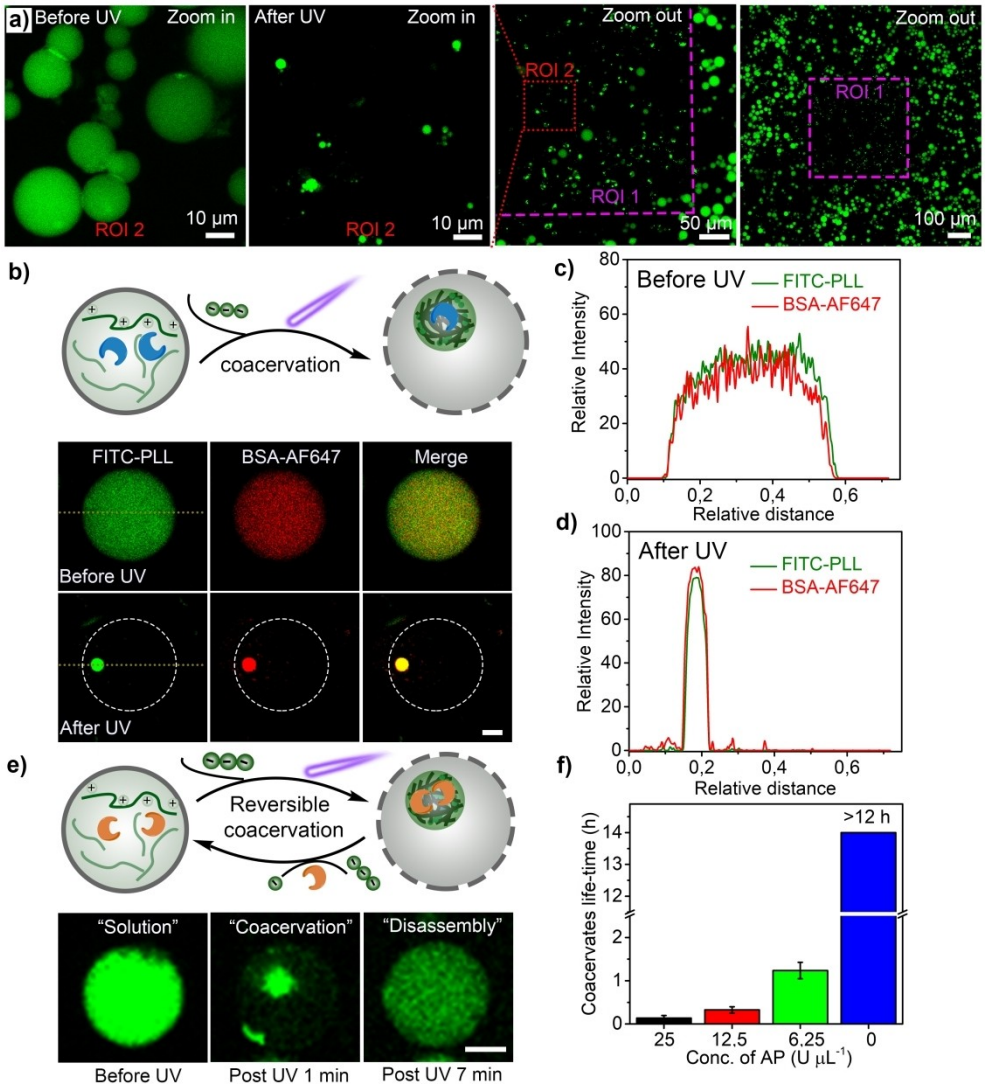

Figure 6. Spatially and temporally regulated coacervation and protein sequestration in SP-GPs. a) Confocal microscopy images showing that coacervation only occurred in areas exposed to UV light. The images are shown in order of increasing field of view. b) The coacervation process inside SP-GPs caused the sequestration of bovine serum albumin (BSA), scale bar = 10 μm. Profile of fluorescent emission intensity of FITC-PLL and BSA c) before and d) after UV irradiation. e) In the presence of co-encapsulated alkaline phosphatase, which hydrolyses ATP, coacervates formed inside the SP-GPs slowly disassembled. f) The lifetime of coacervate droplets inside SP-GPs can be tuned by varying the content of the co-encapsulated enzyme, scale bar = 10 μm.

showed that the coacervate droplets effectively sequester BSA-AF molecules present in the aqueous medium (Figure S30). Next, we tested if the sequestration of BSA-AF could occur inside SP-GPs. To do that, ATP (1 mg mL^{-1}) was added to the external medium of SP-GPs loaded with BSA-AF (0.05 mg mL^{-1}), PLL (10 mg mL^{-1}), and FITC-PLL (0.5 mg mL^{-1}). Before UV irradiation, the distribution of BSA-AF and FITC-PLL within the vesicles was homogeneous (Figure 6b,c). UV irradiation activated the SP-C16 photo-transducer, allowing ATP to cross the vesicle membrane and initiate the coacervation process. The resulting coacervate droplet formed inside the SP-GPs efficiently entrapped BSA-AF (Figure 6b,d, S31). These results demonstrate that cell-like co-localization of biomolecules in biomolecular condensates can be mimicked by synthetic cells constructed using SP-GPs.

The formation of biomolecular condensates in cells is a dynamic process. Their formation and disintegration depend on the concentration of local components, which is constantly changing in response to adaptive cellular processes. Coacervates can mimic some features of such cellular adaptation because their formation and disintegration can be reversibly manipulated by changing the physicochemical properties of the system. To demonstrate dynamic coacervation within SP-GPs, we designed a simple synthetic cell with a rudimentary internal control system. Our synthetic cell consisted of PLL and alkaline phosphatase (AP) encapsulated within SP-GPs. AP is an enzyme that breaks down ATP into adenosine diphosphate (ADP) and finally into

adenosine monophosphate (AMP). Unlike ATP, ADP and AMP interact weakly with the positively charged PLL and cannot form stable coacervates (Figure S32). As demonstrated in bulk, the presence of AP led to the disintegration of ATP/PLL coacervates (Figure S33).

The ATP/PLL coacervates formed inside SP-GPs in the absence of AP were found to be stable for at least 12 h (Figure S34). To induce coacervate disintegration, the SP-GPs were loaded with different concentrations of AP together with PLL ($10\,mg\,m^{-1}$) and FITC-PLL ($0.5\,mg\,mL^{-1}$). The coacervate formation was achieved by incubating the SP-GPs in an ATP-rich solution ($0.5\,mg\,mL^{-1}$) under UV irradiation for 20 s. Confocal imaging showed that the presence of internal AP ($25\,U\,\mu L^{-1}$) did not prevent the onset of coacervation (Figure 6e), with coacervates being observed in the first minute after UV irradiation. Thereafter, the coacervates gradually began to dissolve and returned to the solubilized state ≈ 7 min after UV irradiation (Figure 6e, S35, S36). Lower AP concentrations slowed the ATP hydrolysis process, which increased the lifetime of internal coacervates (Figure 6f). This allowed the lifetime of the coacervates to be modulated from ≈ 10 min to ≈ 1 h depending on the AP concentration.

Conclusion

We have shown that giant polymersomes with light-activated membrane permeability can be used as active compartments for engineering cell-like systems. Photoisomerization of spiropyran photo-transducers was used to create perturbations in the membrane of the polymer vesicles, leading to their effective permeabilization. As a result, the polymersomes exhibited light-activated permeability to small molecules ($MW < 4$ kDa). The photoactivated giant polymersomes discussed in this work are excellent synthetic compartments suitable for the development of robust cell-like structures with controlled molecular membrane transport. This was demonstrated by the development of two different synthetic cells whose internal processes could be regulated by light-induced permeabilization of the polymeric compartments. The internal processes investigated in this work included the control of internal enzymatic reactions and triggered the formation of transient subcompartments within the synthetic cells. The use of polymeric compartments allowed the creation of dynamic systems that exhibit excellent biomimetic utility. We anticipate that the basic design principle of this work will be useful in facilitating the bottom-up fabrication of artificial structures with increasing biological complexity for biotechnological applications.

Acknowledgements

We would like to thank Tsvetomir Ivanov for his support. S.C. thanks the Alexander von Humboldt Foundation for a fellowship and financial grant (No. 3.5-CHN-1222717-HFST-P). This work is part of the research conducted within the Max Planck Consortium for Synthetic Biology (MaxSynBio) jointly funded by the Federal Ministry of Education and Research of Germany (BMBF) and the Max Planck Society. Open Access funding enabled and organized by Projekt DEAL.

Conflict of Interest

The authors declare no conflict of interest.

Data Availability Statement

The data that support the findings of this study are available from the corresponding author upon reasonable request.

Keywords: Coacervates · Light-Activation · Multi-Compartments · Polymersomes · Synthetic Cells

[1] a) P. Tanner, P. Baumann, R. Enea, O. Onaca, C. Palivan, W. Meier, *Acc. Chem. Res.* **2011**, *44*, 1039–1049; b) S. P. Cao, Y. F. Xia, J. X. Shao, B. B. Guo, Y. Y. Dong, I. A. B. Pijpers, Z. Y. Zhong, F. H. Meng, L. Abdelmohsen, D. S. Williams, J. C. M. van Hest, *Angew. Chem. Int. Ed.* **2021**, *60*, 17629–17637; *Angew. Chem.* **2021**, *133*, 17770–17778; c) H. Che, S. Cao, J. C. M. van Hest, *J. Am. Chem. Soc.* **2018**, *140*, 5356–5359; d) Y. Zhu, B. Yang, S. Chen, J. Du, *Prog. Polym. Sci.* **2017**, *64*, 1–22.

[2] a) E. Rideau, R. Dimova, P. Schwille, F. R. Wurm, K. Landfester, *Chem. Soc. Rev.* **2018**, *47*, 8572–8610; b) Y. Tu, F. Peng, A. Adawy, Y. Men, L. K. E. A. Abdelmohsen, D. A. Wilson, *Chem. Rev.* **2016**, *116*, 2023–2078; c) E. Rideau, F. R. Wurm, K. Landfester, *Polym. Chem.* **2018**, *9*, 5385–5394; d) M. Houbrechts, L. Caire da Silva, A. Ethirajan, K. Landfester, *Soft Matter* **2021**, *17*, 4942–4948; e) C. G. Palivan, R. Goers, A. Najer, X. Zhang, A. Car, W. Meier, *Chem. Soc. Rev.* **2016**, *45*, 377–411; f) J. R. Howse, R. A. L. Jones, G. Battaglia, R. E. Ducker, G. J. Leggett, A. J. Ryan, *Nat. Mater.* **2009**, *8*, 507–511.

[3] a) M. Marguet, C. Bonduelle, S. Lecommandoux, *Chem. Soc. Rev.* **2013**, *42*, 512–529; b) L. Schoonen, J. C. M. van Hest, *Adv. Mater.* **2016**, *28*, 1109–1128.

[4] a) T. Trantidou, M. Friddin, Y. Elani, N. J. Brooks, R. V. Law, J. M. Seddon, O. Ces, *ACS Nano* **2017**, *11*, 6549–6565; b) V. Balasubramanian, B. Herranz-Blanco, P. V. Almeida, J. Hirvonen, H. A. Santos, *Prog. Polym. Sci.* **2016**, *60*, 51–85.

[5] a) B. C. Ma, L. C. da Silva, S. M. Jo, F. R. Wurm, M. B. Bannwarth, K. A. I. Zhang, K. Sundmacher, K. Landfester, *ChemBioChem* **2019**, *20*, 2593–2596; b) S. Jiang, L. C. da Silva, T. Ivanov, M. Mottola, K. Landfester, *Angew. Chem. Int. Ed.* **2022**, *61*, 202113784; *Angew. Chem.* **2022**, *134*, 202113784; c) T. Einfalt, M. Garni, D. Witzigmann, S. Sieber, N. Baltisberger, J. Huwyler, W. Meier, C. G. Palivan, *Adv. Sci.* **2020**, *7*, 1901923; d) S. Thamboo, A. Najer, A. Belluati, C. von Planta, D. L. Wu, I. Craciun, W. Meier, C. C. Palivan, *Adv. Funct. Mater.* **2019**, *29*, 1904267.

[6] a) J. C. Blain, J. W. Szostak, *Annu. Rev. Biochem.* **2014**, *83*, 615–640; b) B. C. Buddingh', J. C. M. van Hest, *Acc. Chem. Res.* **2017**, *50*, 769–777; c) C. Xu, S. Hu, X. Chen, *Mater. Today* **2016**, *19*, 516–532; d) C. Guindani, L. Caire da Silva, S. Cao, T. Ivanov, K. Landfester, *Angew. Chem. Int. Ed.* **2022**, *61*, 202110855; *Angew. Chem.* **2022**, *134*, 202110855; e) W. Mu, Z. Ji, M. Zhou, J. Wu, Y. Lin, Y. Qiao, *Sci. Adv.* **2021**, *7*,

eabf9000; f) N.-N. Deng, W. T. S. Huck, *Angew. Chem. Int. Ed.* **2017**, *56*, 9736–9740; *Angew. Chem.* **2017**, *129*, 9868–9872; g) R. Booth, Y. Qiao, M. Li, S. Mann, *Angew. Chem. Int. Ed.* **2019**, *58*, 9120–9124; *Angew. Chem.* **2019**, *131*, 9218–9222.

[7] a) Y. F. Lyu, C. C. Wu, C. Heinke, D. Han, R. Cai, I. T. Teng, Y. Liu, H. Liu, X. B. Zhang, Q. L. Liu, W. H. Tan, *J. Am. Chem. Soc.* **2018**, *140*, 6912–6920; b) Z. W. Chen, J. Q. Wang, W. J. Sun, E. Archibong, A. R. Kahkoska, X. D. Zhang, Y. Lu, F. S. Ligler, J. B. Buse, Z. Gu, *Nat. Chem. Biol.* **2018**, *14*, 86–93; c) J. Steinkuhler, R. L. Knorr, Z. L. Zhao, T. Bhatia, S. M. Bartelt, S. Wegner, R. Dimova, R. Lipowsky, *Nat. Commun.* **2020**, *11*, 905; d) M. Weiss, J. P. Frohnmayer, L. T. Benk, B. Haller, J. W. Janiesch, T. Heitkamp, M. Borsch, R. B. Lira, R. Dimova, R. Lipowsky, E. Bodenschatz, J. C. Baret, T. Vidakovic-Koch, K. Sundmacher, I. Platzman, J. P. Spatz, *Nat. Mater.* **2018**, *17*, 89–96; e) S. Song, A. F. Mason, R. A. J. Post, M. De Corato, R. Mestre, N. A. Yewdall, S. Cao, R. W. van der Hofstad, S. Sanchez, L. K. E. A. Abdelmohsen, J. C. M. van Hest, *Nat. Commun.* **2021**, *12*, 6897; f) B. C. Buddingh', J. Elzinga, J. C. M. van Hest, *Nat. Commun.* **2020**, *11*, 1652; g) Y. Qiao, M. Li, R. Booth, S. Mann, *Nat. Chem.* **2017**, *9*, 110–119.

[8] a) R. J. R. W. Peters, M. Marguet, S. Marais, M. W. Fraaije, J. C. M. van Hest, S. Lecommandoux, *Angew. Chem. Int. Ed.* **2014**, *53*, 146–150; *Angew. Chem.* **2014**, *126*, 150–154; b) E. C. dos Santos, A. Belluati, D. Necula, D. Scherrer, C. E. Meyer, R. P. Wehr, E. Lörtscher, C. G. Palivan, W. Meier, *Adv. Mater.* **2020**, *32*, 2004804.

[9] a) J. W. Hindley, Y. Elani, C. M. McGilvery, S. Ali, C. L. Bevan, R. V. Law, O. Ces, *Nat. Commun.* **2018**, *9*, 1093; b) M. Li, R. L. Harbron, J. V. M. Weaver, B. P. Binks, S. Mann, *Nat. Chem.* **2013**, *5*, 529–536; c) S. D. Pritzl, P. Urban, A. Prasselsperger, D. B. Konrad, J. A. Frank, D. Trauner, T. Lohmuller, *Langmuir* **2020**, *36*, 13509–13515; d) X. Huang, M. Li, D. C. Green, D. S. Williams, A. J. Patil, S. Mann, *Nat. Commun.* **2013**, *4*, 2239.

[10] a) T. Nishimura, S. Hirose, Y. Sasaki, K. Akiyoshi, *J. Am. Chem. Soc.* **2020**, *142*, 154–161; b) H. Niederholtmeyer, C. Chaggan, N. K. Devaraj, *Nat. Commun.* **2018**, *9*, 5027; c) J. Garamella, S. Majumder, A. P. Liu, V. Noireaux, *ACS Synth. Biol.* **2019**, *8*, 1913–1920.

[11] a) R. Merindol, A. Walther, *Chem. Soc. Rev.* **2017**, *46*, 5588–5619; b) N. A. Yewdall, A. F. Mason, J. C. M. van Hest, *Interface Focus* **2018**, *8*, 20180023; c) A. Samanta, V. Sabatino, T. R. Ward, A. Walther, *Nat. Nanotechnol.* **2020**, *15*, 914–921; d) T. Chakraborty, S. V. Wegner, *ACS Nano* **2021**, *15*, 9434–9444.

[12] a) A. Peyret, E. Ibarboure, A. Tron, L. Beauté, R. Rust, O. Sandre, N. D. McClenaghan, S. Lecommandoux, *Angew. Chem. Int. Ed.* **2017**, *56*, 1566–1570; *Angew. Chem.* **2017**, *129*, 1588–1592; b) M. Marguet, L. Edembe, S. Lecommandoux, *Angew. Chem. Int. Ed.* **2012**, *51*, 1173–1176; *Angew. Chem.* **2012**, *124*, 1199–1202; c) A. J. Miller, A. K. Pearce, J. C. Foster, R. K. O'Reilly, *ACS Cent. Sci.* **2021**, *7*, 30–38.

[13] R. Lentini, N. Yeh Martín, S. S. Mansy, *Curr. Opin. Chem. Biol.* **2016**, *34*, 53–61.

[14] L. Caire da Silva, S. Cao, K. Landfester, *ACS Macro Lett.* **2021**, *10*, 401–405.

[15] I. Yildiz, S. Impellizzeri, E. Deniz, B. McCaughan, J. F. Callan, F. M. Raymo, *J. Am. Chem. Soc.* **2011**, *133*, 871–879.

[16] R. Klajn, *Chem. Soc. Rev.* **2014**, *43*, 148–184.

[17] J. G. S. Moo, S. Presolski, M. Pumera, *ACS Nano* **2016**, *10*, 3543–3552.

[18] a) N. A. Yewdall, A. A. M. André, T. Lu, E. Spruijt, *Curr. Opin. Colloid Interface Sci.* **2021**, *52*, 101416; b) S. Koga, D. S. Williams, A. W. Perriman, S. Mann, *Nat. Chem.* **2011**, *3*, 720–724.

[19] a) Y. Shin, C. P. Brangwynne, *Science* **2017**, *357*, eaaf4382; b) W. J. Altenburg, N. A. Yewdall, D. F. M. Vervoort, M. H. M. E. van Stevendaal, A. F. Mason, J. C. M. van Hest, *Nat. Commun.* **2020**, *11*, 6282; c) A. F. Mason, B. C. Buddingh', D. S. Williams, J. C. M. van Hest, *J. Am. Chem. Soc.* **2017**, *139*, 17309–17312.

[20] a) S. Deshpande, F. Brandenburg, A. Lau, M. G. F. Last, W. K. Spoelstra, L. Reese, S. Wunnava, M. Dogterom, C. Dekker, *Nat. Commun.* **2019**, *10*, 1800; b) C. Love, J. Steinkühler, D. T. Gonzales, N. Yandrapalli, T. Robinson, R. Dimova, T.-Y. D. Tang, *Angew. Chem. Int. Ed.* **2020**, *59*, 5950–5957; *Angew. Chem.* **2020**, *132*, 6006–6013.

Manuscript received: April 11, 2022
Accepted manuscript online: June 27, 2022
Version of record online: July 13, 2022